Probing the Thompson Model: Linear Attenuation Coefficients of Aluminium from Na-22, Cs-137, Ba-133, Gamma Rays

Rio Weil*
Department of Physics, University of Chicago, Chicago, Illinois 60637, USA
(Dated: April 4, 2025)

We use a NaI(Ti) crystal coupled to a photomultiplier tube to detect gamma rays from Sodium-22, Cesium-137, and Barium-133 sources. Using high-precision count rate data obtained by fitting pulse-height analyzer outputs at various thicknesses of aluminium shielding, we deduce the linear attenuation coefficient for the material at various energies assuming the Thompson model of scattering. We find 7 best-fit linear attenuation coefficients of $\lambda_{\text{Na}}^{511\text{keV}} = 0.2068(\pm 0.0065)\text{cm}^{-1}$, $\lambda_{\text{Na}}^{1.2\text{MeV}} = 0.137(\pm 0.021)\text{cm}^{-1}$, $\lambda_{\text{Cs}}^{32\text{keV}} = 2.32(\pm 0.10)\text{cm}^{-1}$, $\lambda_{\text{Cs}}^{662\text{keV}} = 0.2032(\pm 0.0090)\text{cm}^{-1}$, $\lambda_{\text{Ba}}^{31\text{keV}} = 2.37(\pm 0.27)\text{cm}^{-1}$, $\lambda_{\text{Ba}}^{81\text{keV}} = 0.429(\pm 0.021)\text{cm}^{-1}$, and $\lambda_{\text{Ba}}^{382\text{keV}} = 0.291(\pm 0.038)\text{cm}^{-1}$.For high energy gammas, we find that the attenuation coefficients for 3 out of 4 tested energies exhibit agreement with literature values, providing evidence that the Thompson model may provide a good description at higher energies. We find the low energy attenuation coefficients to be in tension or disagree with literature values, and conjecture that this may be due to absorption mechanisms such as the photoelectric effect that are not accounted for in the model.

I. INTRODUCTION

High-precision counting experiments are a cornerstone of high-energy experimental physics, being a setting where theories about particles/nuclei can be compared and tested. Scattering experiments are a prominent subset of such experiments, and have been used to probe atomic structure, DNA, and various fundamental particles. In this report, we conduct a tabletop high-precison counting/scattering experiment of our own to test the limits of the Thompson model, a simple classical model for scattering. We will use count rate data across a range of gamma ray energies and absorption thicknesses to extract and compare the cross section/linear attenuation coefficient of alumnium to accepted literature values, and see where the model succeeds and where it breaks down.

The rest of this paper is organized as follows. In section II, we review the Thompson model of scattering and also introduce the quantum-mechanical models of scattering/absorption that proceed it. In section III we discuss the experimental apparatus and how the raw data was collected. In section IV we display/characterize the pulse height analyzer spectra and explain the fitting procedure for obtaining count data from the raw spectral data. In section V we discuss and show the results of the fitting procedure for obtaining the linear attenuation coefficient for alumnium for each of the probed gamma ray energies. In section VI we compare these coefficients to tabulated literature values. In section VII we discuss the dominant absorption mechanisms for our probed energy scales and conclude with what our data tells us about limitations of the Thompson model.

* ryoheiweil@uchicago.edu

II. THEORY

In the classical Thompson model of scattering, we consider a beam of gamma rays of intensity R incident on a slab of area A thickness dx. Assuming the slab has electron density N and effective interaction area per electron of σ (the cross-section), the fraction of the slab covered by electrons, and hence the probability of gamma ray scattering is given by:

$$\frac{NAdx\sigma}{A} = N\sigma dx \tag{1}$$

Hence after passing through the slab, we expect a decrease in density:

$$dR = -N\sigma dx R \tag{2}$$

which we can integrate to obtain a thickness dependent rate:

$$R(x) = R_0 e^{-N\sigma x} = R_0 e^{-\lambda x} \tag{3}$$

where in the last equality we define the linear attenuation coefficient $\lambda = N\sigma$, which is an energy and material dependent quantity. In the proceeding sections, we will measure a gamma rays over a range of energies at various absorption thicknesses x to extract λ from the Thompson model.

It is worth noting that the Thompson model is a classical, incomplete theory. A more complete contemporary understanding of material cross sections involves three (quantum-mechanical) effects/processes:

- Compton scattering, wherein a photon collides with an electron in the material and loses energy. This is relevant at all energy scales.
- The photoelectric effect, wherein a photon is fully absorbed by an atom, liberating an electron. This is relevant at low energy (keV)/binding energy scales.

- Pair production, where a photon spontaneously decays into an electron-positron pair. This is relevant at high energy (MeV)/at energies greater than double the mass energy of an electron.

We will return to a discussion of which of the three absorption processes are dominant for each of the studied gamma-ray energies in the conclusions section of the paper.

III. APPARATUS + DATA COLLECTION

In this experiment, we use Na-22, Cs-137, and Ba-133 as radioactive sources of gamma rays. To measure these gamma rays, we use a detector consisting of a NaI(Ti) crystal coupled to a photomultiplier tube (PMT) to produce an amplified output voltage pulse proportional to the energy deposited in the crystal from the gamma ray emitted from the source. We then use the *USX* program to interface with a pulse-height analyzer (PHA) which collects pulses from the PMT and displays a histogram of pulse sizes. More precisely, from the PHS we can read out the number of counts/pulses associated to a given energy channel, which is again proportional to the incoming photon energy (we take the measured quantity of pulse counts to be a proxy for gamma ray counts). This provides a histogram/spectra which is the raw data upon which our analysis is based.

Between the detector (crystal + PMT) and source, we place aluminium absorption shielding. We place the shielding such that the midpoint is located halfway between the source and the detector, so as to minimize the competing effects of (a) gamma rays missing the shielding and going directly into the detector and (b) gamma rays scattering into the detector when they would have missed it initially. We dynamically adjust the height of the shielding as we change the thickness to maintain this good geometry. A diagram of the experimental setup is below:

For absorption shielding, we used a series of aluminium plates of increasing thickness (~ 0.5mm, ~ 1mm, ~ 2mm up to ~ 64mm). The plate thicknesses were measured via calipers, and the uncertainty in the thicknesses were estimated from the instrumental precision/resolution (0.05mm). We stacked plates as necessary to collect data spaced out relatively evenly over the range of thicknesses, in order to better characterize the exponential decay of the count rate for each gamma ray energy (over approximately one decade of count rate).

For each peak, we started by conducting a multi-minute run to characterize the spectra and determine the region of interest corresponding to each peak, as we discuss in the next section. We took this to be the range of channels over which the peak was distinguishable - until the tails of the Gaussian had decayed into the background. This procedure for choosing the region of interest was done such that the Gaussian fitting parameters would yield an accurate estimation of the number of counts associated to a given gamma ray energy.

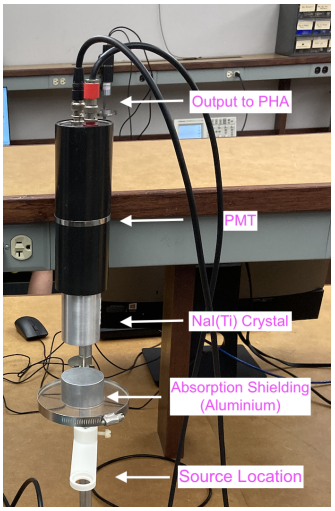

FIG. 1. Diagram of setup of source, shielding, and crystal/PMT detector.

For each peak (at each thickness of absorption shielding), we collected counts until there were > 4000 counts under a given peak, so as to minimize statistical uncertainty within the time allotted. For a given energy channel that registered counts, we assume the number of gamma particles N counted in a given time interval is described by Poisson statistics, and so the statistical uncertainty in the counts is given by $\sqrt{N}$. To obtain the rate, we also recorded the live counting time (total time minus detector dead time) as measured by the *USX* software, which has an uncertainty of $\pm 0.5s$ (half of the smallest measurable time interval by the counter of 1 second).

IV. SPECTRA + PEAK FITTING

For each of the three types of radioactive sources, we collected a spectrum of zero absorption to identify relevant features in the spectrum (via reference to known nuclear decay schemes) and identify peaks/gamma ray energies of interest. These are displayed and discussed for the three sources, below.

For the Sodium spectrum in Fig 2, the dominant peak (green) in channels [311, 391] is identified as the 511keV peak, and the other relevant peak (blue) in channels [789, 905] is identified as the 1.2MeV peak. For each peak, we identify a Compton edge/shelf (orange/red) corresponding to events where the gamma rays Compton scatter once before hitting the detector (with the edge corresponding to maximum energy transfer/scattering angle of 180°). We also identify a backscatter peak (purple) arising from photons which scatter off the table top and then pass back through the source into the detector. By eye, it can be verified that the sum of the compton edge

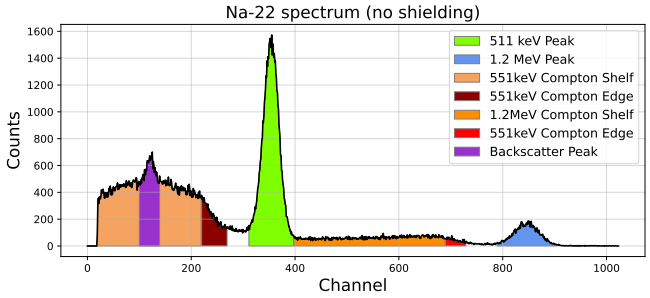

FIG. 2. Counts vs. Energy spectrum for Na-22 with no shielding/absorption. Data was collected with a PMT high voltage of 1000V and a PHA coarse/fine gain of 2x/1.5x, for 183 seconds.

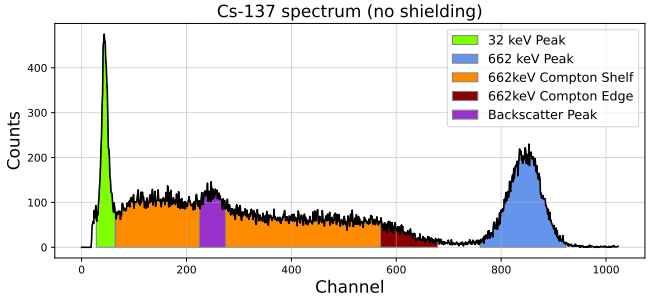

FIG. 3. Counts vs. Energy spectrum for Cs-137 with no shielding/absorption. Data was collected with a PMT high voltage of 1000V and a PHA coarse/fine gain of 4x/1.5x, for 244 seconds.

energy and the backscatter peak energy match up with the energy of the full peaks.

For the Cesium spectrum in Fig 3, the dominant peak (green) in channels [28, 65] is identified as the 32keV peak, and the other dominant peak (blue) in channels [760, 925] is identified as the 662keV peak. For the 662keV peak, we identify a Compton edge/shelf (orange/red). We also identify a backscatter peak (purple), and can again verify that the sum of the Compton edge energy and the backscatter peak energy matches up with the location of the 662keV peak.

Finally, for the Barium spectrum in Fig 4, the dominant peak (green) in channels [69, 101] is identified as the 31keV peak, and a sub-dominant peak (blue) in channels [184, 253] is identified as the 81keV peak (though there is also a 79keV decay mode for which the peak has overlap). At higher energies we observe broadened peaks arising from a combination of decay modes - there is a more prominent peak (pink) in channels [790, 960] which we identify as the 382keV peak, with contributions from the 356keV decay mode. There is also a supressed peak (orange) arising from the 276keV and 302keV decay modes which we considered too suppressed to fit/extract the count rate. Finally, we observe a small bump (purple) which we conjecture to be a backscatter peak.

We wish to obtain the number of counts associated to

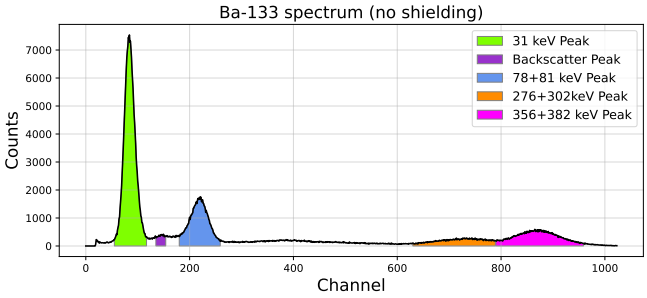

FIG. 4. Counts vs. Energy spectrum for Ba-133 with no shielding/absorption. Data was collected with a PMT high voltage of 1000V and a PHA coarse/fine gain of 8x/1.5x, for 299 seconds.

a given gamma ray energy - to this end, to each distinguishable/dominant peak (of which we have 7 in total - 511keV and 1.2MeV for Sodium, 32keV and 662keV for Cesium, and 31keV, 81keV, and 382keV for Barium) in the above spectra we fit a Gaussian with linear background (to account for possible asymmetry from other features in the spectrum):

$$f(x) = \frac{N}{\sqrt{2\pi}} e^{-\frac{(x-\mu)^2}{2\sigma^2}} + mx + b \tag{4}$$

To illustrate, in Fig. 5 we display the fit and residuals for the 662keV peak of Cesium.

The linear least squares fit yields a reduced chi-squared of $\chi_r^2 \approx 1$, suggesting a good fit with appropriately estimated uncertainties. This is further supported by the residuals, which exhibit random scatter that would be expected from a normally distributed random variable. We repeat this fitting procedure for each of the 7 peaks of interest across the 3 radiation sources for each absorption thickness measured, and in each case obtain a reduced χ_r^2 of $0.8 < \chi_r^2 < 1.6$, indicating a good fit/reasonable uncertainty estimation.

V. EXTRACTING LINEAR ATTENUATION COEFFICIENTS

Having obtained the number of counts $N \pm dN$ for each energy peak (varying the absorption thickness), we can then divide by the live time $t \pm dt$ to obtain the count rate $R(x)$ for the specific gamma ray energy at thickness x. The uncertainty in N is obtained from the peak fit parameters, and $dt = 0.5$s from instrumental resolution. The uncertainty in $R(x)$ is obtained by adding relative uncertainties in quadrature:

$$dR = R\sqrt{\left(\frac{dN}{N}\right)^2 + \left(\frac{dt}{t}\right)^2} \tag{5}$$

The dominant uncertainty in dR arises from $\frac{dN}{N}$. $\frac{dt}{t}$ is on the order of fractions of a percent, as we take count data

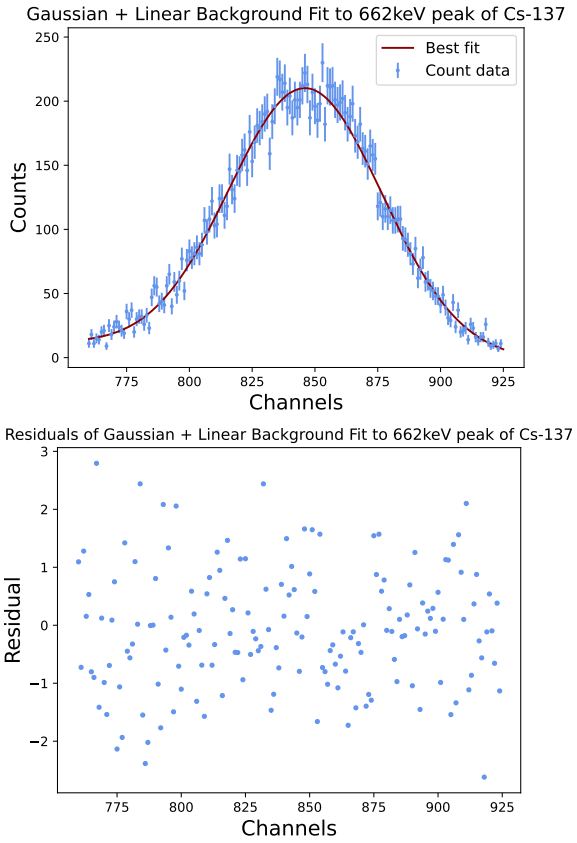

FIG. 5. Count data of 662keV peak of Cesium, taken for $t = 244 \pm 0.5$s at 0 absorption, displayed with best fit line (using the model of Eq. (4) for channels $760 - 925$), and corresponding plot of residuals. The best fit parameters were obtained to be $N = 1.572(\pm 0.025) \times 10^4$, $\mu = 846.32(\pm 0.35)$, $\sigma = 30.52(\pm 0.42)$, $m = -0.071(\pm 0.011)$, $b = 65.0(\pm 8.9)$. The fit converged with a reduced chi-squared of $\chi_r^2 = 1.09$.

over hundreds of seconds, while the relative uncertainty in the peak count of N can on the order of a few percent. Both terms can be decreased by taking longer counting periods/increasing both N and t. Although the plate thicknesses also carry uncertainty, these are negligible in comparison to the uncertainty in the rate, so we neglect them in the fitting procedure (we do include them in the later plots, but in all cases they are too small to be visible).

Having then obtained $R(x) \pm dR(x)$ across a range of thicknesses, we then fit the R vs. x curve with the exponential fitting function:

$$g(x) = R_0 e^{-\lambda x} + b \tag{6}$$

Therein, R_0 represents the count rate at zero thickness, λ the linear attenuation coefficient, and b a constant which accounts for counts from constant background sources. From this we can obtain the linear attenuation coefficient for each gamma ray energy. To this end, in Figs 6 - 12 we display the count rate data, uncertainties, and best fits with parameters.

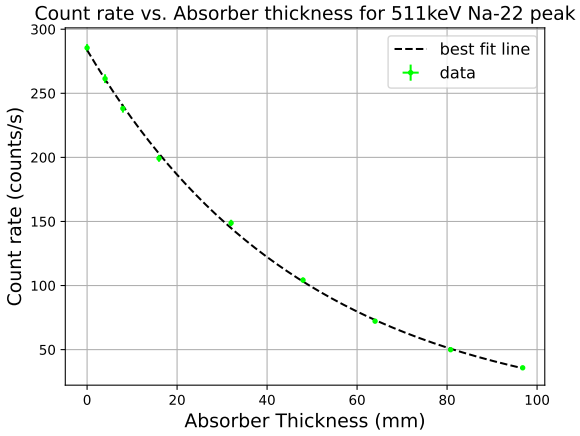

FIG. 6. Fitted count rate vs. absorption thickness for 551keV peak of Na-22, displayed with best fit (using the model of Eq. (6)). The best fit parameters were obtained to be $\lambda = 0.2068(\pm 0.0065)\text{cm}^{-1}$, $R_0 = 287.1(\pm 3.0)$counts/s, $b = -3.3(\pm 3.3)$counts/s. The fit converged with a reduced chi-squared of $\chi_r^2 = 1.07$. Where not visible, error bars are behind markers.

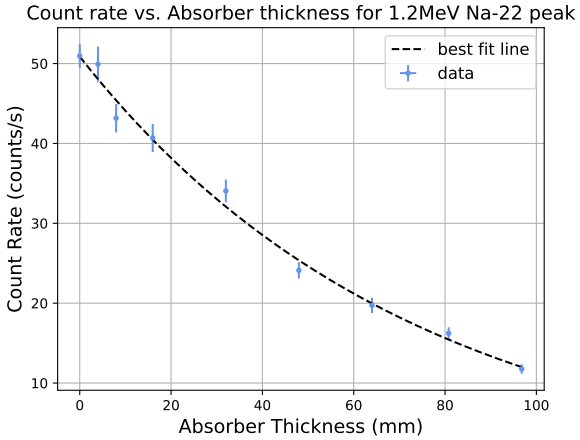

FIG. 7. Fitted count rate vs. absorption thickness for 1.2MeV peak of Na-22, displayed with best fit (using the model of Eq. (6)). The best fit parameters were obtained to be $\lambda = 0.137(\pm 0.021)\text{cm}^{-1}$, $R_0 = 52.9(\pm 3.9)$counts/s, $b = -2.0(\pm 4.3)$counts/s. The fit converged with a reduced chi-squared of $\chi_r^2 = 1.18$.

In the next section, we summarize the linear attenuation coefficients and associated uncertainties as obtained by the least squares fitting, and compare to literature values (see Table I). Before proceeding, we first discuss some anomalies in the data/observations acquired during data collection and fitting.

First, we observed for the low energy peaks (namely Cesium's 32keV and Barium's 31keV) that above shielding of 16mm the peaks were no longer observable from the background, even when taking data on the order of 10 minutes or longer. There are two possible explana-

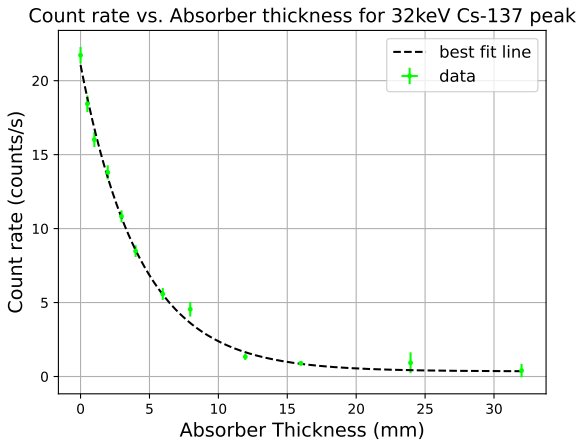

FIG. 8. Fitted count rate vs. absorption thickness for 32keV peak of Cs-137, displayed with best fit (using the model of Eq. (6)). The best fit parameters were obtained to be $\lambda = 2.32(\pm 0.10)\text{cm}^{-1}$, $R_0 = 20.71(\pm 0.36)$counts/s, $b = 0.34(\pm 0.17)$counts/s. The fit converged with a reduced chi-squared of $\chi^2_r = 1.21$.

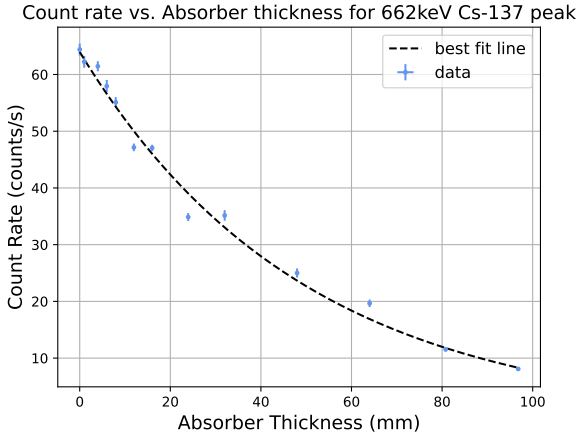

FIG. 9. Fitted count rate vs. absorption thickness for 662keV peak of Cs-137, displayed with best fit (using the model of Eq. (6)). The best fit parameters were obtained to be $\lambda = 0.2032(\pm 0.0090)\text{cm}^{-1}$, $R_0 = 64.72(\pm 0.82)$counts/s, $b = -0.7(\pm 1.0)$counts/s. The fit converged with a reduced chi-squared of $\chi^2_r = 9.43$.

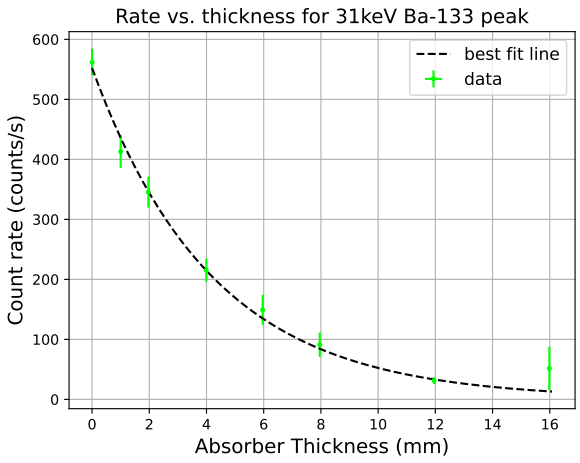

FIG. 10. Fitted count rate vs. absorption thickness for 31keV peak of Ba-133, displayed with best fit (using the model of Eq. (6)). The best fit parameters were obtained to be $\lambda = 2.37(\pm 0.27)\text{cm}^{-1}$, $R_0 = 551(\pm 19)$counts/s, $b = 0.8(\pm 13)$counts/s. The fit converged with a reduced chi-squared of $\chi^2_r = 0.51$.

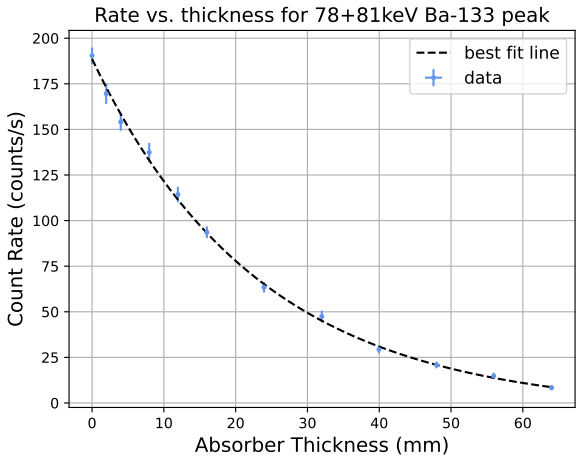

FIG. 11. Fitted count rate vs. absorption thickness for 81keV peak of Ba-133, displayed with best fit (using the model of Eq. (6)). The best fit parameters were obtained to be $\lambda = 0.429(\pm 0.021)\text{cm}^{-1}$, $R_0 = 192.4(\pm 3.0)$counts/s, $b = -3.7(\pm 2.5)$counts/s. The fit converged with a reduced chi-squared of $\chi^2_r = 0.49$. When not visible, error bars are behind markers.

tions - either we are in the near-zero tail of the exponential (and low energy gammas attenuate much quicker) or above some absorption thickness a different physical process may prohibit the transmission of gamma rays in any meaningful capacity. To combat this, we took more finely spaced data over thinner absorption thicknesses as to better characterize the entire exponential curve, as can be seen in Figs. 8, 10.

On the other hand, for high energy peaks (such as Sodium's 1.2MeV and Cesium's 662keV), we do not see an appreciable decay in the count rate for small amounts of shielding. We interpret this to mean that high-energy gamma rays have a smaller linear attenuation coefficient, and as such to fully characterize/see the exponential decay of the count rate we took data out to high thicknesses by stacking multiples of the highest thickness absorbers, as can be seen in Figs. 7, 9.

Another observation concerning the model function we used for fitting - In basically all cases, the best fit value for b is small, and/or the uncertainty in b is the same order as/larger than b. This suggests that background counts from external sources are negligible. Indeed, we

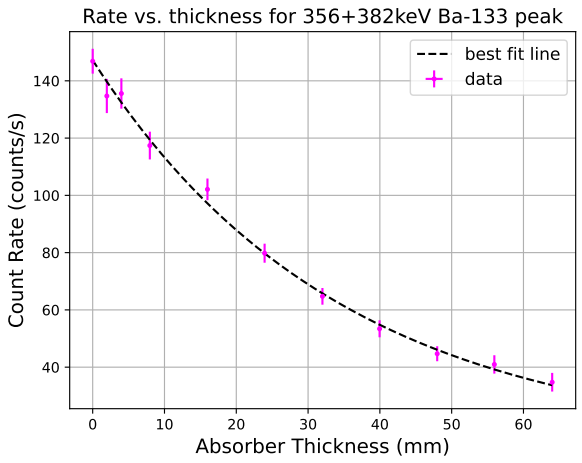

FIG. 12. Fitted count rate vs. absorption thickness for 1.2MeV peak of Ba-382, displayed with best fit (using the model of Eq. (6)). The best fit parameters were obtained to be $\lambda = 0.291(\pm 0.038)\text{cm}^{-1}$, $R_0 = 134.3(\pm 7.1)$counts/s, $b = 12.8(\pm 7.9)$counts/s. The fit converged with a reduced chi-squared of $\chi^2_r = 0.49$.

may remove this parameter from the model without impacting its ability to well-describe the data (and in fact, removing this parameter may lead to a better goodness of fit/less overconstraining).

Analyzing the goodness of fit, we notice that $\chi^2_r \sim 1$ for both sodium peaks as well as the 32keV Cesium peak. This suggests a good fit with well-estimated uncertainties. The 662keV peak for Cesium instead has a $\chi^2_r = 9.42$, suggesting that the uncertainties may have been underestimated in this case (this is supported by analyzing the best fit plot, where the error bars look quite small and the majority do not intersect the best fit line). Finally, for the three Barium peaks, we have $\chi^2_r \sim 0.5$ which suggests that uncertainties may have been slightly overestimated. It is worth noting that the Barium spectrum was less clean and many of the features involved the overlap of multiple peaks. For future experiments, we may consider increasing the waiting time/number of counts in order to decrease the uncertainty in the rate to decrease uncertainties and better constrain the fit.

VI. COMPARISON TO LITERATURE VALUES

We use the provided literature values of linear attenuation coefficients as converted from the NIST FAAST and XAAMDI databases to compare with our results. We assume the uncertainty in the literature values are negligible. We match each measured peak to the closest literature value, taking averages of literature values as necessary. In table I we tabulate our results, the corresponding literature values, and the statistical t-score:

$$t' = \frac{\lambda_{\text{exp}} - \lambda_{\text{lit}}}{d\lambda_{\text{exp}}} \tag{7}$$

Source	Peak	$\lambda_{\text{exp}}(\text{cm}^{-1})$	Lit. Energy	$\lambda_{\text{lit}}(\text{cm}^{-1})$	t'
Na	511keV	0.2068($\pm$0.0065)	500keV	0.2275	-3.16
Na	1.2MeV	0.137($\pm$0.021)	1250keV	0.1481	-0.498
Cs	32keV	2.32($\pm$0.10)	32.09keV	2.5482	-2.22
Cs	662keV	0.2032($\pm$0.0090)	600+800keV	0.1972	0.66
Ba	31keV	2.37($\pm$0.27)	30.01+32.09keV	2.7807	-1.52
Ba	81keV	0.429($\pm$0.021)	81.66keV	0.5397	-5.38
Ba	382keV	0.291($\pm$0.038)	378.86keV	0.2596	0.83

TABLE I. Linear attenutation coefficeints obtained experimentally from Thompson model, literature (NIST) values, and comparisons.

between the two.

For the 1.2MeV Sodium peak, 662keV Cesium peak, and 382keV Barium peak, we have $|t'| < 1$ and so we are not at all confident the experimental value and literature value are different (i.e. they are consistent).

For the Cesium 32keV, Barium 31keV, and 382 keV peaks, $1 < |t'| < 3$ and so the results are in statistical tension. A more precise estimation of the experimental linear attenuation coefficients would be able to resolve the tension, and either reveal a difference or allow us to conclude consistency with the literature values. Note that a t'-score between the Cesium 32keV and Barium 31keV results yields $t' = -0.18$, showing the two results are consistent (as we might expect, for gamma rays of similar energies).

Finally, the Sodium 511keV and Barium 81keV peaks have $|t'| > 3$, so we are confident that the experimental value and the literature value are different. We discuss possible reasons for the discreptancy in the next section.

VII. IDENTIFYING ABSORPTION MECHANISMS + CONCLUSIONS

We used the Thompson model to fit and extract linear attenuation coefficients, but the linear attenuation of Aluminium is now understood to be based on a combination of Compton scattering, the photoelectric effect, and pair production, as shown in Fig. 13

Let us discuss the implications of this plot for the gamma ray energies studied in our experiment. First, we note that none of the studied energies we studied in this experiment were larger than the $\sim$ 2MeV threshold above which pair production effects become relevant. We thus only consider effects from Compton scattering and the photoelectric effect.

For the high energy peaks studied (both sodium peaks, 662keV peak of Cesium, and 382keV peak of Barium) the photoelectric effect has negligible contribution to the linear attenuation coefficient, and thus the dominant absorption mechanism comes from Compton scattering. For sodium and the cesium peak this is further supported by the characteristics in the spectrum data, where we could observe a Compton shelf/edge for the high energy

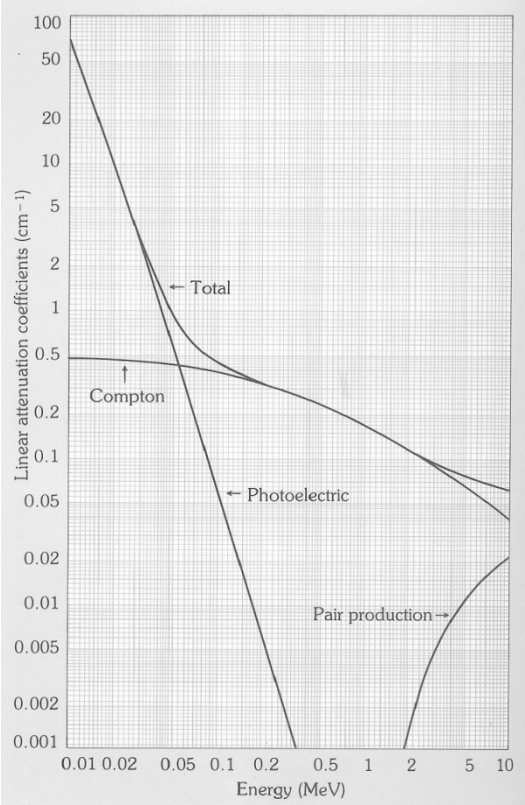

FIG. 13. Plot of various contributions to the linear attenuation coefficient of Aluminium across a range of energies. Plot reproduced without permission from Harshaw Radiation Detectors Catalog.

peaks. It is also worth noting that (with the notable exception of the 511keV Na peak), all of the high energy peaks demonstrated agreement with literature values for the linear attenuation coefficient. This suggests that the Thompson model is a reasonable model for describing the scattering of high-energy photons from aluminium.

However, our value for the 511keV sodium gamma does cast some doubt onto this conclusion, as for this peak we see that the linear attenuation is statistically significantly lower than the literature value. One possibility is that (as we can see from the spectrum) the compton shelves of the 511keV/1.2MeV) peaks appear to "leak in" to the 511keV peak, possibly leading to an overestimation of the number of 511keV events and thus count rate when fitting the data (Though in principle the linear background term should take care of such leakage, so this seems unlikely). It may also be possible that a fitting model that took more carefully into account the physics of Compton scattering would predict a higher amount of absorption than the Thompson model. In any case, further exploration of count rates at this energy would be valuable for greater confidence that this is a datapoint where the model fails, and the reason for the discreptancy.

For the low energy gammas, the photoelectric effect becomes a significant contributor to the linear attenuation coefficient, with the 31/32keV gammas of Barium/Cesium having the photoelectric effect as the dominant mode of absorption, and it being a significant contributor to the absorption of the 81keV peak of Barium (though Compton scattering is still the dominant mode of absorption in this case, by a factor of 2). Indeed we see in all three of these cases that the linear attenuation value as obtained from experiment assuming the Thompson model is smaller than the literature value, by 1.5-5 standard deviations. We conjecture that probing absorption at small energies exposes a shortcoming of the Thompson model, and if we were to add the photoelectric effect into our model that we may obtain a more accurate value of the linear attenuation coefficient.

In conclusion, we have used the Thompson model of scattering to extract the linear attenuation coefficient of aluminium across 7 gamma ray energies from 3 different sources. The uncertainties in the coefficients we obtain are small enough for a high precision test of the model. At high energies, 3 out of 4 coefficients exhibit agreement with literature values. 1 of the high energy coefficients and all 3 low energy coefficients disagree or are in statistical tension with literature values, and we suspect that this may arise from an incomplete account of absorption mechanisms, namely the photoelectric effect in the low energy case.

DATA AVAILABILITY

All `.tsv` files of raw data, as well as the Jupyter notebook used for data analysis + display of the results can be find in the attached `rioscatter.zip` archive, submitted along with this report.

ACKNOWLEDGMENTS

We wish to acknowledge Aashay Pai for coding help for displaying of spectrum data. The 334 lab wiki was used liberally in the structuring of the background of this report.